

Excitation energies from frozen-density embedding with accurate embedding potentials

Denis G. Artiukhin,¹ Christoph R. Jacob,^{2,a)} and Johannes Neugebauer^{1,b)}

¹Theoretische Organische Chemie, Organisch-Chemisches Institut and Center for Multiscale Theory and Computation, Westfälische Wilhelms-Universität Münster, Corrensstraße 40, 48149 Münster, Germany

²Institute of Physical and Theoretical Chemistry, TU Braunschweig, Hans-Sommer-Straße 10, 38106 Braunschweig, Germany

(Received 25 February 2015; accepted 1 June 2015; published online 15 June 2015)

We present calculations of excitation energies within the time-dependent density functional theory (TDDFT) extension of frozen-density embedding (FDE) using reconstructed accurate embedding potentials. Previous applications of FDE showed significant deviations from supermolecular calculations; our current approach eliminates one potential error source and yields excitation energies of generally much better agreement with Kohn–Sham-TDDFT. Our results demonstrate that the embedding potentials represent the main error source in FDE-TDDFT calculations using standard approximate kinetic-energy functionals for excitations localized within one subsystem. © 2015 AIP Publishing LLC. [<http://dx.doi.org/10.1063/1.4922429>]

I. INTRODUCTION

Frozen-density embedding (FDE) is an embedding scheme within density-functional theory (DFT) that utilizes a density partitioning into an active and an environmental system.¹ The effective embedding potential for the active part is derived from a minimization of the total energy with respect to the density of the active system (ρ_{act}), assuming that the density of the environment (ρ_{env}) is fixed. It reads

$$v_{\text{emb}}(\mathbf{r}) = v_T^{\text{nadd}}[\rho_{\text{act}}, \rho_{\text{env}}](\mathbf{r}) + v_{\text{xc}}^{\text{nadd}}[\rho_{\text{act}}, \rho_{\text{env}}](\mathbf{r}) - \sum_{A \in \text{env}} \frac{Z_A}{|\mathbf{r} - \mathbf{R}_A|} + \int \frac{\rho_{\text{env}}(\mathbf{r}')}{|\mathbf{r} - \mathbf{r}'|} d\mathbf{r}', \quad (1)$$

where the last two terms are the electrostatic potentials due to the nuclei in the environment (with charges Z_A at positions \mathbf{R}_A) and the environment's electron density. The non-additive kinetic-energy potential is given as

$$v_T^{\text{nadd}}[\rho_{\text{act}}, \rho_{\text{env}}](\mathbf{r}) = \left. \frac{\delta T_s[\rho]}{\delta \rho(\mathbf{r})} \right|_{\rho=\rho_{\text{act}}+\rho_{\text{env}}} - \left. \frac{\delta T_s[\rho]}{\delta \rho(\mathbf{r})} \right|_{\rho=\rho_{\text{act}}}, \quad (2)$$

and the non-additive exchange-correlation (XC) potential $v_{\text{xc}}^{\text{nadd}}[\rho_{\text{act}}, \rho_{\text{env}}]$ is defined analogously. $T_s[\rho]$ is the non-interacting kinetic-energy functional as defined in the context of Kohn–Sham DFT (KS-DFT).

By iteratively exchanging active system and environment in so-called freeze-and-thaw cycles,² a fully self-consistent subsystem DFT solution is obtained (for a recent review, see Ref. 3). Excited-state generalizations of FDE and subsystem DFT in the context of time-dependent density-functional theory (TDDFT) have been proposed and implemented.^{4–6} An overview and discussion of electronic-spectra calculations with FDE are provided in Refs. 7 and 8. While several applications of FDE-TDDFT to local excitations of an active subsystem were very successful,^{5,9–11} not all solvent-induced

shifts as calculated from supermolecular TDDFT could quantitatively be reproduced.^{8,12,13} There are several possible error sources that could explain this observation. (i) FDE-TDDFT calculations usually employ only the basis functions of the active subsystem. Tests indicate, however, that using the full supermolecular basis only leads to modest changes in typical applications.^{12,13} Note, however, that using a supermolecular basis may lead to charge-leaking (also known as overpolarization) effects.^{14,15} (ii) Usually, the response is restricted to the active system. This means that inter-subsystem transitions are ignored, and that the response contribution of the environment is neglected. Neglecting couplings between excitations localized in the active system and the environment is often a good approximation, unless near-degeneracies occur. However, attempts to include environment response or polarization effects either in terms of direct response couplings^{8,13} or through state-specific embedding potentials in the context of related wavefunction-in-DFT embedding^{16,17} did not in general lead to satisfactory agreement with supermolecular results. (iii) An approximation is needed for the non-additive kinetic-energy potential (and kernel in case of TDDFT) for which usually local-density approximation (LDA) or generalized-gradient approximation (GGA) potentials are employed. The approximation for the non-additive XC-functional is usually not such a problem, as the same approximation as in the supermolecular case can be employed (unless orbital-dependent XC-functionals are used).

Issue (iii) mentioned above has received comparatively little attention in the literature. It can be anticipated that the non-additive kinetic energy contributions will be the more important, the larger the density overlap of the two subsystems is. In an analysis in Ref. 13, it was shown that for longer distances between the subsystems even completely neglecting the non-electrostatic contributions to the embedding potential yields excitation energies in near-perfect agreement with supermolecular TDDFT. At shorter distances, however, the non-additive contributions become more important, and the

^{a)}Electronic mail: c.jacob@tu-braunschweig.de

^{b)}Electronic mail: j.neugebauer@uni-muenster.de

agreement with the supermolecular reference usually gets worse. Reconstructing accurate embedding potentials offers a possibility for assessing the error due to approximations in the non-additive kinetic energy.^{18–22} We use this technique here to correct FDE-TDDFT for errors in the embedding potential. We only consider errors in the non-additive kinetic-energy potential, as errors in the non-additive XC potential will be made consistently in FDE and supermolecular Kohn–Sham DFT calculations.

The present study is intended as a proof-of-principle showing that accurate local embedding potentials can be constructed and applied for the calculation of excitation energies. This will be useful both for future work on the development of approximate, analytical non-additive kinetic-energy potentials (following, e.g., similar strategies as in the design of exchange-correlation potentials^{23,24}) and for use in combined wavefunction/DFT hybrid methods. A first approximate step towards the latter goal was very recently made by Roncero *et al.*²⁵ Moreover, already for FDE-TDDFT calculations, the approach employed here can offer computational advantages. The embedded excitation-energy calculations themselves are computationally cheap compared to the supermolecular alternative, since they involve the reduced occupied-virtual space of the embedded subsystem only. Furthermore, the spectra obtained are much cleaner,⁹ since, for example, mixings with inter-subsystem charge-transfer (CT) states, which are described incorrectly with many exchange-correlation approximations,^{26–29} are avoided. The construction of an accurate embedding potential in our present setup, however, requires the calculation of a supermolecular reference density. Still, the supermolecular TDDFT part of the calculation is avoided.

II. METHODOLOGY

The reconstruction used here follows our earlier work in Ref. 19: We first perform a supermolecular KS-DFT calculation on the microsolvated complex. As an exchange-correlation potential (for intra- and inter-subsystem contributions), we consistently use the Perdew–Wang functional denoted as PW91.^{30,31} The triple-zeta basis set including one set of polarization functions for all atoms (TZP) from the ADF basis set library is used in all cases. From this calculation, we construct a set of localized orbitals $\{\psi_i^{\text{loc}}\}$ using the Boys–Foster algorithm,³² where the localization ensures that the orbitals have non-negligible contributions only on one of the subsystems. This means that we can write this set of orbitals as the union of two sets of orbitals localized on either the active system or the environment,

$$\{\psi_i^{\text{loc}}\} = \{\psi_i^{\text{loc,act}}\} \cup \{\psi_i^{\text{loc,env}}\}. \quad (3)$$

For the embedding calculations, we construct an environmental density as

$$\rho_{\text{env}}(\mathbf{r}) = \sum_i^{N_{\text{env}}} |\psi_i^{\text{loc,env}}(\mathbf{r})|^2 \quad (4)$$

(with N_{env} being the number of electrons in the environment), so that the target density for the active region in the FDE calculation is $\rho_{\text{act}}^{\text{target}} = \rho_{\text{tot}} - \rho_{\text{env}}$. This choice ensures that

$\rho_{\text{act}}^{\text{target}}$ is non-negative everywhere in space, which is a prerequisite for non-interacting v -representability.

For the embedding potential in Eq. (1), an approximate expression for v_T^{nadd} is needed in addition to exchange-correlation approximations, which are also necessary in the KS context. As explained in detail in Ref. 19, we can numerically reconstruct a formally exact v_T^{nadd} up to a constant shift as

$$v_T^{\text{nadd}}(\mathbf{r}) = v_s[\rho_{\text{act}}](\mathbf{r}) - v_s[\rho_{\text{tot}}](\mathbf{r}), \quad (5)$$

where $v_s[\rho_{\text{input}}](\mathbf{r})$ is the local potential that has the given input density ρ_{input} as its non-interacting ground-state density. For the potential reconstruction, the potential that should reproduce the target density is expressed as

$$v_s(\mathbf{r}) = v_0(\mathbf{r}) + \sum_t b_t g_t(\mathbf{r}). \quad (6)$$

Here, $v_0(\mathbf{r})$ is an initial guess potential, which in our case is calculated from the isolated fragment densities $\rho_{\text{act}}^{\text{iso}}$ and $\rho_{\text{env}}^{\text{iso}}$ as ($v_{\text{KS}}[\rho_{\text{act}}^{\text{iso}}](\mathbf{r})$ denotes the usual Kohn–Sham potential of the isolated active system)

$$v_0(\mathbf{r}) = v_{\text{KS}}[\rho_{\text{act}}^{\text{iso}}](\mathbf{r}) + v_{\text{emb}}[\rho_{\text{act}}^{\text{iso}}, \rho_{\text{env}}^{\text{iso}}](\mathbf{r}) \quad (7)$$

$$= - \sum_{A \in \text{act}} \frac{Z_A}{|\mathbf{r} - \mathbf{R}_A|} + \int \frac{\rho_{\text{act}}^{\text{iso}}(\mathbf{r}')}{|\mathbf{r} - \mathbf{r}'|} d\mathbf{r}' + v_{\text{xc}}[\rho_{\text{act}}^{\text{iso}}](\mathbf{r}) \\ + v_T^{\text{nadd}}[\rho_{\text{act}}^{\text{iso}}, \rho_{\text{env}}^{\text{iso}}](\mathbf{r}) + v_{\text{xc}}^{\text{nadd}}[\rho_{\text{act}}^{\text{iso}}, \rho_{\text{env}}^{\text{iso}}](\mathbf{r}) \\ - \sum_{A \in \text{env}} \frac{Z_A}{|\mathbf{r} - \mathbf{R}_A|} + \int \frac{\rho_{\text{env}}^{\text{iso}}(\mathbf{r}')}{|\mathbf{r} - \mathbf{r}'|} d\mathbf{r}', \quad (8)$$

where the PW91 approximation^{30,31} is applied for the exchange-correlation potential and the non-additive exchange-correlation potential. For the non-additive kinetic-energy potential, the so-called PW91k approximation is employed here.^{33,34}

The second term in Eq. (6) consists of unknown coefficients b_t (initially zero) and basis functions $g_t(\mathbf{r})$. We use the same set of basis functions that is employed as an auxiliary basis for the fitted electron density in ADF and which is taken from the standard ADF basis set library.³⁵ Note that we directly reconstruct the *total* effective single-particle potential for the target subsystem density $\rho_{\text{act}}^{\text{target}}$ here. In other words, neither v_T^{nadd} nor the embedding potential v_{emb} from Eq. (1) is explicitly constructed. They could, of course, be derived from the total potential and the knowledge of the effective Kohn–Sham potential for the supermolecular density. Also note that orbital-dependent XC-potentials (e.g., in hybrid DFT methods) would introduce an additional complication, since they are usually combined with (semi-)local non-additive XC-potentials; as an alternative, an additional potential reconstruction step can be used.³⁶

Although formally exact, it has to be kept in mind that a numerical reconstruction is performed, and no analytical density-dependent expression is obtained. Moreover, the result will only be as accurate as possible within the limitations³⁷ of the numerical reconstruction algorithms used for obtaining $v_s[\rho_{\text{input}}](\mathbf{r})$. The term $v_s[\rho_{\text{tot}}](\mathbf{r})$ equals the effective Kohn–Sham potential of the total system and can be obtained in a straightforward way from a supermolecular KS-DFT calculation. For $v_s[\rho_{\text{act}}](\mathbf{r})$, we follow Ref. 19 and

reconstruct this term numerically for $\rho_{\text{act}} = \rho_{\text{act}}^{\text{target}}$ by means of the Wu–Yang method.³⁸ We apply a regularization norm as suggested in Ref. 39 and used in Ref. 19, which is added to the Lagrangian functional with a weight parameter $\lambda = 0.001$ (if not mentioned otherwise) chosen on the basis of initial test calculations. This additional term ensures the smoothness of the reconstructed potential in case of non-unique reconstructed potentials. We confirmed by test calculations that the HOMO–LUMO gap, taken as an indicator for the excitation energy, remains stable over hundreds of iteration cycles with this setting. By contrast, calculations without this smoothing ($\lambda = 0$) started deteriorating under the same conditions. All our calculations are carried out using a development version of the program package ADF.^{35,40}

Concerning the computational cost, the calculation time will be dominated by the calculation of the supermolecular density if the environment is large. For the present examples, however, the supermolecular systems are not much larger than the active systems. Therefore, the actual optimization of the expansion coefficients for the potential can take a considerable part of the total time for these specific examples and is comparable to the time needed in the TDDFT step of the active system. But more importantly, the cost for this potential optimization step is determined by the size of the active subsystem, whereas the cost for the reference-density calculation depends on the size of the total system (for details, see Ref. 19).

We then carry out a FDE–TDDFT calculation using the orbitals and orbital energies obtained in this way, together with the adiabatic local density approximation (ALDA), which in case of FDE implies a Thomas–Fermi (TF)–like kinetic-energy contribution to the response kernel.^{3,5} For comparison, we also report data obtained with approximate non-additive kinetic-energy potentials. Either the TF approximation or the so-called PW91k approximation has been applied in that case.^{33,34} All FDE–TDDFT calculations have been carried out in the so-called “uncoupled FDE” or FDEu approximation,^{6,8} first introduced in Ref. 5, and alternatively known as the “neglect of differential response of the environment” (NDRE) approximation.¹⁰ For the calculations with reconstructed potentials, the terms in the exchange–correlation–kinetic-energy kernel are approximately evaluated with the electron densities of the isolated subsystems. Tests without the embedding contribution in the exchange–correlation kernel confirm that these contributions are very small, even at the shortest distances considered here.

All equilibrium structures have been optimized in supermolecular Kohn–Sham calculations using the Becke–Perdew exchange–correlation functional.^{41,42}

III. RESULTS

As a test system, we consider the singlet $\pi \rightarrow \pi^*$ transition in a complex of 2-aminopyridine (active system) and methanol (environment), see Figures 1(a) and 1(b). Significant solvent effects have been observed for this system in the excited-state studies in Ref. 43. Starting from the optimized structure, we increased the distance between the two molecules along the O···H hydrogen bond while keeping the monomer structures fixed. The excitation energies as a function of

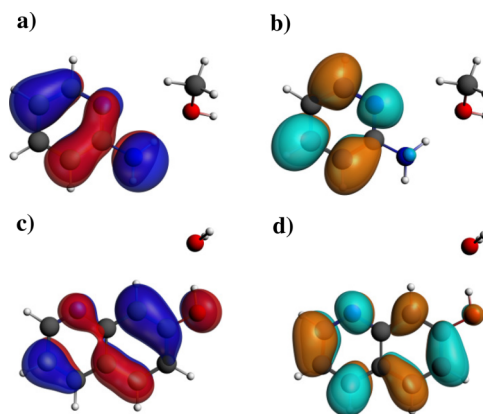


FIG. 1. Isosurface plots (isosurface value: ± 0.03 a.u.) of π and π^* orbitals involved in the electronic transitions of the 2-aminopyridine···methanol complex (a) and (b) and the *cis*-7-hydroxyquinoline···H₂O complex (c) and (d) studied here.

the displacement from the reference structure are shown in Figure 2 (top). It can clearly be seen that FDE calculations using the PW91k potential for $v_T^{\text{nadd}}(\mathbf{r})$ underestimate the solvent-induced red-shift at short distances. At the equilibrium distance, the unrelaxed (i.e., no freeze-and-thaw) FDE excitation energy is 0.044 eV higher than the supermolecular reference. The error decreases to 0.026 eV if relaxation is accounted for in terms of freeze-and-thaw cycles. Using the Thomas–Fermi approximation for the non-additive kinetic energy leads to similar, though slightly better results. At the equilibrium distance, the errors compared to the supermolecular reference are 0.040 and 0.023 eV without and with relaxation, respectively.

For the potential reconstruction, one usually carries out the optimization of the Lagrangian in the Wu–Yang scheme until the density drops below a certain threshold. Because

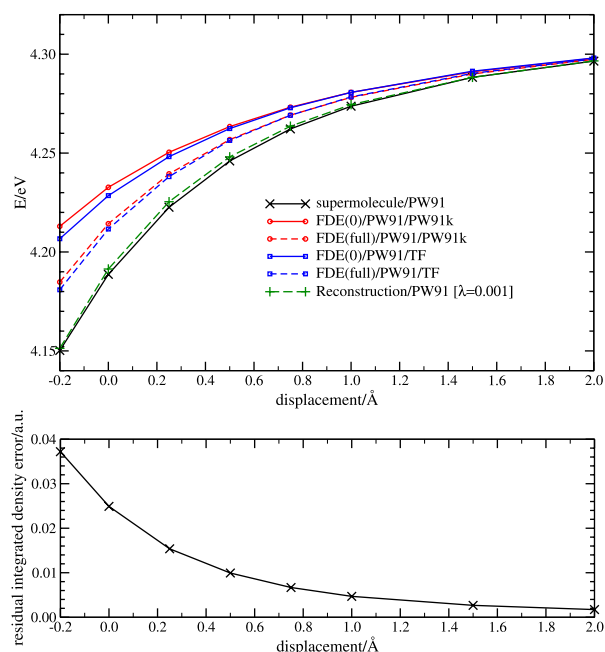


FIG. 2. Top: Excitation energy of the lowest singlet $\pi \rightarrow \pi^*$ transition in the 2-aminopyridine···methanol complex as a function of the hydrogen-bond displacement. FDE(0) refers to unrelaxed environment densities and FDE(full) denotes full mutual relaxation. Bottom: Residual integrated density error in the potential reconstruction.

of orthogonality tails in the target density (due to the orbital localization step), a residual density error usually has to be accepted, especially if only a monomer basis in the active system is employed.^{3,19} In our current study concerning excitation-energy curves, this residual error is distance dependent. Initial tests indicated, however, that the density error as a function of the iteration count in the Wu–Yang scheme behaves qualitatively very similar for all distances of the system studied here. It rapidly decreases during the first 10–20 iterations, after which a stable residual density error is reached. Hence, we decided to consider a potential reconstruction converged if the change in the density error between two subsequent iterations is smaller than a threshold of 1%. The residual integrated density errors obtained with this criterion as a function of the displacement from the equilibrium distance are shown in the lower panel of Figure 2, and decrease from 0.037 a.u. at a displacement of -0.2 Å to less than 0.002 at 2 Å. With this procedure, we arrive at excitation energies that are much better than the ones obtained with approximate analytical functional expressions for the non-additive kinetic-energy potentials. At the equilibrium distance, the error compared to the supermolecular calculation is as small as 0.003 eV.

We would like to note that there are still several error sources, which point to the possibility that the excellent agreement observed here is at least partially due to error cancellation effects. For example, we only use a monomer basis set in our calculations, while the reference results are obtained with a supermolecular basis. In Fig. 3, we report additional results obtained for the 2-aminopyridine \cdots CH₃OH system employing supermolecular basis sets in the embedding calculations. Results are shown for approximate kinetic-energy potentials based on the PW91k expression, as well as for reconstructed potentials. Compared to the results with monomer basis sets in Fig. 2, all embedding curves are shifted to lower excitation energies. This makes the agreement better for the approximate potentials, but leads to an underestimation of the excitation energies by the reconstruction scheme. Still, reconstruction yields the smallest deviations from the reference energies (<0.01 eV even at the shortest distance).

As a second example, we study the case of *cis*-7-hydroxyquinoline \cdots H₂O, which was also investigated in

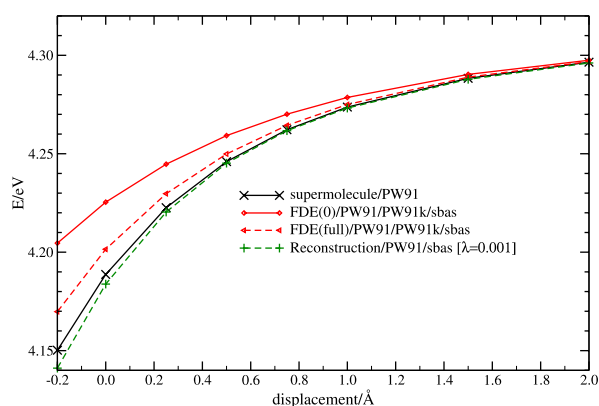


FIG. 3. Excitation energy of the lowest singlet $\pi \rightarrow \pi^*$ transition in the 2-aminopyridine \cdots methanol complex using a supermolecular basis (sbas). FDE(0) refers to unrelaxed environment densities and FDE(full) denotes full mutual relaxation in terms of freeze-and-thaw cycles.

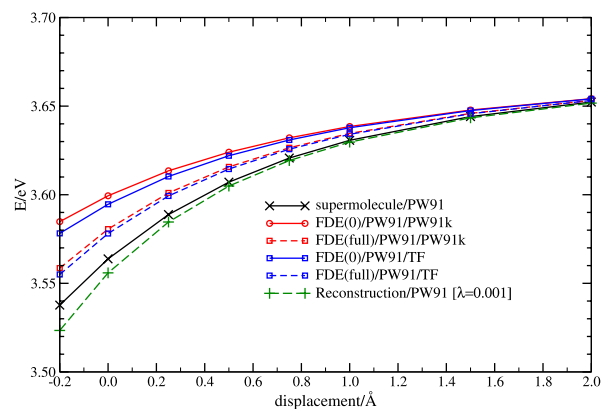


FIG. 4. Excitation energy of the lowest singlet $\pi \rightarrow \pi^*$ transition in the *cis*-7-hydroxyquinoline \cdots H₂O complex as a function of the hydrogen-bond displacement. FDE(0) refers to unrelaxed environment densities, FDE(full) denotes full mutual relaxation in terms of freeze-and-thaw cycles.

Ref. 44 with approximate embedding potentials. Here, the hydroxyquinoline is the active system, while water is considered as the environment. The molecular orbitals involved in the HOMO \rightarrow LUMO ($\pi \rightarrow \pi^*$) transition considered here are shown in Figs. 1(c) and 1(d). The excitation-energy curves as a function of the hydrogen-bond displacement from the equilibrium distance are shown in Fig. 4.

The agreement with the supermolecular reference is excellent for displacements of 0.75 Å and larger, and reconstruction clearly outperforms approximate potentials. At shorter distances, we note that the supermolecular results are slightly underestimated. Nevertheless, the accuracy is still remarkable. For instance, the error at the equilibrium distance is still smaller than 0.01 eV.

If GGA-type exchange-correlation functionals are employed, the neglect of inter-subsystem CT transitions can be considered as an advantage of FDE-TDDFT calculations, as spuriously low long-range CT excitations may obscure the spectra of solvated molecules in supermolecular TDDFT calculations.⁹ But in turn, this means that deviations between FDE (not affected by this problem) and supermolecular Kohn–Sham TDDFT results may be more pronounced, because the latter are not a suitable reference for these excitations. We will demonstrate this effect here for the example of the acetophenone \cdots water complex shown in Fig. 5, where acetophenone represents the active system, and the water

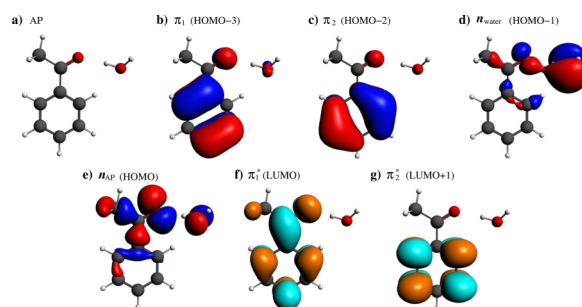


FIG. 5. Structure of the acetophenone \cdots H₂O system (AP) and isosurface plots (isosurface value ± 0.03 a.u.) of the molecular orbitals involved in the lowest five singlet-singlet transitions as obtained in supermolecular PW91/TZP calculations at the equilibrium distance.

molecule is considered the environment. Among the five lowest-lying excited singlet states for this system are, at the equilibrium distance, in energetic order (PW91/TZP): (i) an $n_{\text{AP}} \rightarrow \pi_1^*$ excitation [index “AP” denotes acetophenone], (ii) an intermolecular $n_{\text{water}} \rightarrow \pi_1^*$ CT transition, (iii) a low-intensity $\pi_{(1,2)} \rightarrow \pi_{(1,2)}^*$ excitation, (iv) an $n_{\text{AP}} \rightarrow \pi_2^*$ excitation, and (v) an intense $\pi_{(1,2)} \rightarrow \pi_{(1,2)}^*$ excitation. Isosurface plots of the orbitals involved can be found in Fig. 5. Excitation-energy curves from supermolecular calculations and from FDE are shown in Fig. 6. Already at the equilibrium distance, there

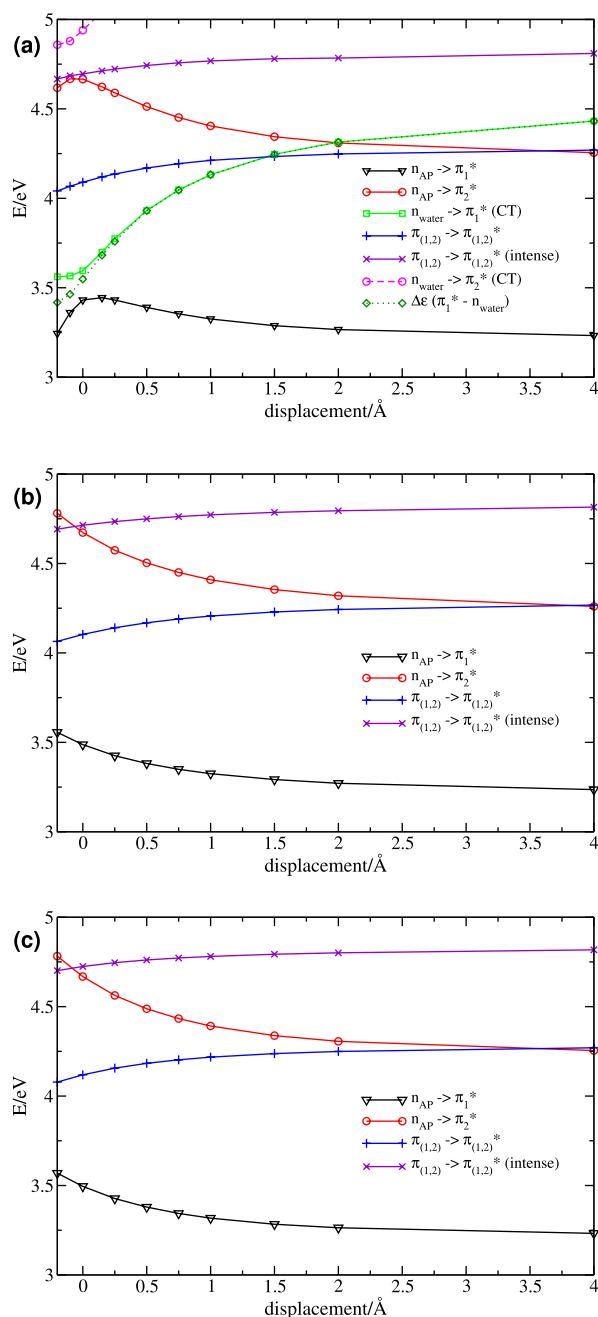


FIG. 6. Excitation energies of the lowest singlet transitions in the acetophenone...water complex as a function of the hydrogen-bond displacement; (a) supermolecular TDDFT (PW91/TZP); for the analysis of the $n_{\text{water}} \rightarrow \pi_1^*$ CT transition, also the corresponding orbital-energy difference $\Delta\epsilon(\pi_1^* - n_{\text{water}})$ is shown, (b) FDE-TDDFT with reconstructed potentials ($\lambda = 0.015$), and (c) FDE-TDDFT with approximate analytical potentials (PW91/PW91k/TZP).

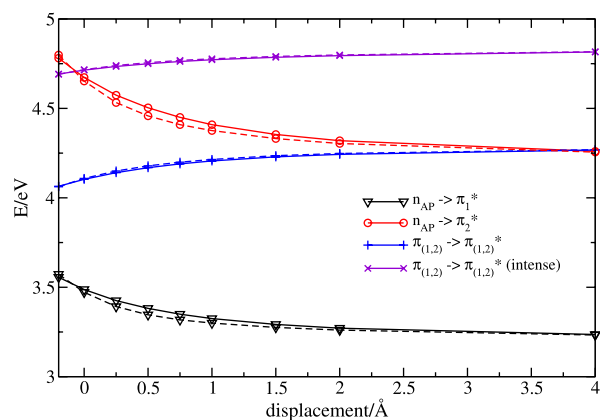


FIG. 7. Excitation energies of the lowest singlet transitions in the acetophenone...water complex as a function of the displacement along the hydrogen bond. Results are shown for FDE-TDDFT with reconstructed potentials and two different values of the smoothing parameter λ : Solid curves: $\lambda = 0.015$ [same as in Fig. 6(b)]. Dashed curves: $\lambda = 0.001$.

is a pronounced delocalization of orbitals between the two systems in the supermolecular case and significant mixing of the orbital transitions within one electronic excitation. This means that the assignment at short distances (equilibrium distance and shorter) is difficult, and higher excited states may become involved. The CT excitation increases in energy with increasing distance, and thereby crosses some of the other states, which again leads to certain mixings of orbital transitions. The fact that this excitation suffers from the typical TDDFT problems for long-range CT transitions (for LDA/GGA) can be seen from the orbital energy difference for the orbitals π_1^* and n_{water} [shown in Fig. 6(a)]. It is virtually identical to the actual CT excitation energy for all but the shortest distances, which is a clear indication of this failure of approximate TDDFT methods (cf. Refs. 26–29).

The FDE results reproduce the supermolecular excitation energies at intermediate distances and give a much clearer picture at short distances, which can actually help for an assignment of the supermolecular results. We note that for this example, the choice of $\lambda = 0.015$ led to better agreement with the supermolecular curve at intermediate distances. A comparison of results obtained with $\lambda = 0.015$ and $\lambda = 0.001$ is shown in Fig. 7. FDE with approximate analytical potentials leads to a similar accuracy in this case [see Fig. 6(c)]. This probably reflects the more difficult potential reconstruction because of the stronger hydrogen-bonding interaction (equilibrium distance here: 1.83 Å compared to 1.99 Å for 2-aminopyridine...water), which leads to stronger mixing of the canonical orbitals and larger orthogonalization tails of the localized orbitals used for constructing the target density. This mixing concerns in particular the non-bonding orbitals (see Fig. 5). Related to this, we note that the $n \rightarrow \pi^*$ transitions react more strongly to the choice of the smoothing parameter λ , as can be seen from the plot in Fig. 7.

IV. CONCLUSIONS

In conclusion, we have shown here that potential reconstruction can be used to obtain accurate excitation energies for local excitations from FDE-TDDFT calculations. Not only

single-points but also entire excitation-energy curves can be well described in this way. The resulting excitation energies are still very accurate at distances corresponding to equilibrium distances (or shorter) of hydrogen-bonded complexes, while the accuracy of explicitly density-dependent potential approximations often deteriorates in that distance regime. On the practical side, we note that the residual density error is of course distance dependent, but the convergence criterion introduced here is suited to generate accurate and smooth excited-state potential-energy surfaces. This residual density error could be removed by obtaining the subsystem densities iteratively instead of relying on localized orbital densities.^{45,46} It should be noted that the remaining density errors found here (even for the shortest distances) are still smaller than the ones obtained for covalently bonded systems in Ref. 19. Whether or not the present scheme can be generalized to such very strongly interacting fragments will be the subject of future investigations.

Concerning additional approximations affecting the excitation energies, we have shown that both the restriction to a monomer basis set and the details of the numerical reconstruction (choice of λ) may introduce non-negligible changes. Further approximations that are made in our calculations concern the exchange-correlation kernel, the assumption of a localized response in the active system, and the neglect of CT effects between the systems.

The approach used here can be computationally attractive if the TDDFT part of the supermolecular calculation becomes the most time-consuming step. Moreover, a pair approximation could be introduced to avoid the full supermolecular ground-state calculation when treating larger solvent environments.⁴⁷ Also, if the analysis of supermolecular TDDFT results is complicated by spurious transitions introduced by approximations in the exchange-correlation potential or kernel, the present setup can help to purify the spectrum while making sure that the short-range interactions are accurately described. More importantly, the present results are encouraging for future work on (i) developing analytical, density-dependent approximations for non-additive kinetic-energy potentials, similar to the corresponding work in the field of exchange-correlation potentials^{23,24} and on (ii) the use of reconstructed accurate potentials in the context of wavefunction-in-DFT embedding for excited states, where a supermolecular DFT calculation as needed for the reconstruction step is of low computational effort compared to a correlated wavefunction calculation on the active part. Here, the simple smoothing applied in the current work might not be appropriate anymore for obtaining sufficiently accurate reconstructed potentials, but more sophisticated schemes are available.^{37,48}

ACKNOWLEDGMENTS

D.G.A. and J.N. acknowledge funding by the Deutsche Forschungsgemeinschaft (DFG), Project No. NE 912/3-1.

¹T. A. Wesolowski and A. Warshel, *J. Phys. Chem.* **97**, 8050 (1993).

²T. A. Wesolowski and J. Weber, *Chem. Phys. Lett.* **248**, 71 (1996).

³C. R. Jacob and J. Neugebauer, *Wiley Interdiscip. Rev.: Comput. Mol. Sci.* **4**, 325 (2014).

⁴M. E. Casida and T. A. Wesolowski, *Int. J. Quantum Chem.* **96**, 577 (2004).

⁵T. A. Wesolowski, *J. Am. Chem. Soc.* **126**, 11444 (2004).

⁶J. Neugebauer, *J. Chem. Phys.* **126**, 134116 (2007).

⁷A. S. P. Gomes and C. R. Jacob, *Annu. Rep. Prog. Chem., Sect. C: Phys. Chem.* **108**, 222 (2012).

⁸J. Neugebauer, in *Recent Progress in Orbital-Free Density Functional Theory*, edited by T. A. Wesolowski and Y. A. Wang (World Scientific, Singapore, 2013), pp. 325–356.

⁹J. Neugebauer, M. J. Louwerse, E. J. Baerends, and T. A. Wesolowski, *J. Chem. Phys.* **122**, 094115 (2005).

¹⁰G. Fradelos, J. W. Kaminski, T. A. Wesolowski, and S. Leutwyler, *J. Phys. Chem. A* **113**, 9766 (2009).

¹¹C. König and J. Neugebauer, *J. Chem. Theory Comput.* **9**, 1808 (2013).

¹²J. Neugebauer, C. R. Jacob, T. A. Wesolowski, and E. J. Baerends, *J. Phys. Chem. A* **109**, 7805 (2005).

¹³A. Kovyrshin and J. Neugebauer, *Chem. Phys.* **391**, 147 (2011).

¹⁴C. R. Jacob, S. M. Beyhan, and L. Visscher, *J. Chem. Phys.* **126**, 234116 (2007).

¹⁵G. Fradelos and T. A. Wesolowski, *J. Phys. Chem. A* **115**, 10018 (2011).

¹⁶C. Daday, C. König, O. Valsson, J. Neugebauer, and C. Filippi, *J. Chem. Theory Comput.* **9**, 2355 (2013).

¹⁷C. Daday, C. König, J. Neugebauer, and C. Filippi, *ChemPhysChem* **15**, 3205 (2014).

¹⁸O. Roncero, M. P. de Lara-Castells, P. Villarreal, F. Flores, J. Ortega, M. Paniagua, and A. Aguado, *J. Chem. Phys.* **129**, 184104 (2008).

¹⁹S. Fux, C. R. Jacob, J. Neugebauer, L. Visscher, and M. Reiher, *J. Chem. Phys.* **132**, 164101 (2010).

²⁰S. Fux, Ch. R. Jacob, J. Neugebauer, L. Visscher, and M. Reiher, *J. Chem. Phys.* **135**, 027102 (2011).

²¹J. D. Goodpaster, N. Ananth, F. R. Manby, and T. F. Miller, *J. Chem. Phys.* **133**, 084103 (2010).

²²C. Huang and E. A. Carter, *J. Chem. Phys.* **135**, 194104 (2011).

²³O. V. Gritsenko, P. R. T. Schipper, and E. J. Baerends, *Chem. Phys. Lett.* **302**, 199 (1999).

²⁴O. V. Gritsenko, P. R. T. Schipper, and E. J. Baerends, *Int. J. Quantum Chem.* **76**, 407 (2000).

²⁵O. Roncero, A. Aguado, F. A. Batista-Romero, M. I. Bernal-Uruchurtu, and R. Hernández-Lamonedá, *J. Chem. Theory Comput.* **11**, 1155 (2015).

²⁶A. Dreuw, J. L. Weisman, and M. Head-Gordon, *J. Chem. Phys.* **119**, 2943 (2003).

²⁷A. Dreuw and M. Head-Gordon, *J. Am. Chem. Soc.* **126**, 4007 (2004).

²⁸O. Gritsenko and E. J. Baerends, *J. Chem. Phys.* **121**, 655 (2004).

²⁹J. Neugebauer, O. Gritsenko, and E. J. Baerends, *J. Chem. Phys.* **124**, 214102 (2006).

³⁰J. P. Perdew, J. A. Chevary, S. H. Vosko, K. A. Jackson, M. R. Pederson, D. J. Singh, and C. Fiolhais, *Phys. Rev. B* **46**, 6671 (1992).

³¹J. P. Perdew, in *Electronic Structure of Solids*, edited by P. Ziesche and H. Eschrig (Akademie Verlag, Berlin, 1991), p. 11.

³²J. M. Foster and S. F. Boys, *Rev. Mod. Phys.* **32**, 300 (1960).

³³A. Lembarki and H. Chermette, *Phys. Rev. A* **50**, 5328 (1994).

³⁴T. A. Wesolowski, H. Chermette, and J. Weber, *J. Chem. Phys.* **105**, 9182 (1996).

³⁵“Amsterdam density functional program,” Theoretical Chemistry, Vrije Universiteit, Amsterdam, URL: <http://www.scm.com>.

³⁶S. Laricchia, E. Fabiano, and F. Della Sala, *Chem. Phys. Lett.* **518**, 114 (2011).

³⁷Ch. R. Jacob, *J. Chem. Phys.* **135**, 244102 (2011).

³⁸Q. Wu and W. Yang, *J. Chem. Phys.* **118**, 2498 (2003).

³⁹F. A. Bulat, T. Heaton-Burgess, A. J. Cohen, and W. Yang, *J. Chem. Phys.* **127**, 174101 (2007).

⁴⁰G. te Velde, F. M. Bickelhaupt, E. J. Baerends, S. J. A. van Gisbergen, C. Fonseca Guerra, J. G. Snijders, and T. Ziegler, *J. Comput. Chem.* **22**, 931 (2001).

⁴¹A. D. Becke, *Phys. Rev. A* **38**, 3098 (1988).

⁴²J. P. Perdew, *Phys. Rev. B* **33**, 8822 (1986).

⁴³J. Hager and S. C. Wallace, *J. Phys. Chem.* **89**, 3833 (1985).

⁴⁴M. Humbert-Droz, X. Zhou, S. V. Shedge, and T. A. Wesolowski, *Theor. Chem. Acc.* **133**, 1405 (2014).

⁴⁵O. Roncero, A. Zanchet, P. Villarreal, and A. Aguado, *J. Chem. Phys.* **131**, 234110 (2009).

⁴⁶C. Huang, M. Pavone, and E. A. Carter, *J. Chem. Phys.* **134**, 154110 (2011).

⁴⁷J. D. Goodpaster, T. A. Barnes, and T. F. Miller, *J. Chem. Phys.* **134**, 164108 (2011).

⁴⁸K. Boguslawski, Ch. R. Jacob, and M. Reiher, *J. Chem. Phys.* **138**, 044111 (2013).